Analytical and Bioanalytical Chemistry
https://doi.org/10.1007/s00216-019-02325-9

RESEARCH PAPER

Fluorescent recognition and selective detection of nitrite ions with carbon quantum dots

Wenshuai Li[1] · Saipeng Huang[1] · Huiyun Wen[1] · Yane Luo[2] · Jiewei Cheng[1] · Zhao Jia[3] · Pu Han[1] · Weiming Xue[1]

Received: 9 October 2019 / Revised: 8 November 2019 / Accepted: 3 December 2019

Abstract

The nitrite ion (NO_2^-) is a vital inorganic species that occurs both in natural ecological systems and human bodies. The high concentration of NO_2^- can be harmful for animal and human health. It is important to develop a simple, sensitive, reliable, and economic methodology to precisely monitor NO_2^- in various environmental and biological fields. Thus, a novel nitrite biosensor based on carbon quantum dots (PA-CDs) has been constructed and prepared via a high-efficiency, one-pot hydrothermal route using primary arylamines (PA) such as *m*-phenylenediamine. The device exhibits bright green fluorescence and a high quantum yield of 20.1% in water. In addition, the PA-CDs also possess two broad linear ranges: 0.05–1.0 μM and 1.0–50 μM with a low detection limit of 7.1 nM. The classical diazo reaction is firstly integrated into the PA-CD system by primary arylamines, which endows the system with high sensitivity and specific selectivity towards nitrite. Importantly, the nanosensor can detect NO_2^- in environmental water and serum samples with high fluorescence recoveries, demonstrating its feasibility in practical applications. This work broadens a new method to fabricate novel nanosensors and provides a prospective application for fluorescent carbon quantum dots (CDs).

Keywords Carbon quantum dots · Nitrite · Diazo reaction · Primary arylamines · Fluorescence

Introduction

Nitrite ions (NO_2^-) are widely used as chemical fertilizing agents and food antiseptics in agriculture and the food industry, respectively. However, trace amounts of nitrite ions can cause severe environmental contamination which can negatively affect human health [1–3]. Due to their chemical versatility and intimate molecular interactions with proteins, NO_2^- ions play important roles as precursors for the generation of highly carcinogenic N-nitrosamines by combining with amides/amines [4, 5]. Nitrite ions can cause hemoglobin to permanently lose its blood oxygen-carrying capacity upon irreversible oxidation [6]. For example, the most common form of blue baby syndrome, a serious congenital heart defect, is caused by an excessive dose of NO_2^- and successive inadequate blood oxygen-transporting capacity [7]. Hence, excessive consumption and accumulation of nitrites in human bodies can cause a series of diseases, such as infant methemoglobinemia, esophageal cancer, spontaneous miscarriage, and birth defects in the central nervous system. Besides, endogenous nitrite in biological systems (such as serum samples) is a crucial chemical signal source for vasodilator nitric oxide [8], which plays a significant role in metabolic functions, such as the regulation of vascular tone [9], neurotransmitters [10], and others.

The US Environmental Protection Agency (EPA) has set the maximum contaminant level (MCL) of NO_2^- at 1 ppm (or 21.7 μM), and an analogous guideline value of 3 ppm (or 65 μM) has been set by the World Health Organization (WHO) [11]. Therefore, it is vital to develop a simple, sensitive, reliable, economical, and green methodology to precisely monitor NO_2^- in a variety of environments. Such a method

Electronic supplementary material The online version of this article (https://doi.org/10.1007/s00216-019-02325-9) contains supplementary material, which is available to authorized users.

✉ Saipeng Huang
huangsaipeng@nwu.edu.cn

✉ Weiming Xue
xue_wm@126.com

[1] School of Chemical Engineering, Northwest University, Xi'an 710069, Shaanxi, China

[2] College of Food Science and Technology, Northwest University, Xi'an 710069, China

[3] Shangluo University, Shangluo 726000, Shaanxi, China

Published online: 13 January 2020

will have profound significance and practical value for environmental monitoring and human clinical diagnoses. A wide variety of analytical techniques for nitrite detection have been developed in the last decade, including electrochemical methods [12], capillary electrophoresis [13], electrochemiluminescence [14], chromatography [15], Raman spectrometry [16], molecular absorption spectrometry [17], and chemiluminescence [18]. Despite these advances, most of these methods require tedious treatment procedures, expensive equipment, and high costs. They also have low detection limits and sensitivities, which greatly hinder their practical applications. Compared with the above technologies, fluorescent carbon quantum dots are promising nanomaterials that possess numerous attractive properties, including easy preparation, low cost, great photoluminescence, outstanding photostability, high water solubility, and low toxicities [19–21]. Due to these excellent features and advantages, carbon quantum dots are strong candidates for the development of novel, stable, and sensitive nanosensors. In the last decade, carbon quantum dots have been widely utilized as direct fluorescence indicators for metal ions [22–24], while few carbon quantum dots have been used to detect nitrite ions.

Herein, a methodology has been developed for using novel carbon quantum dots (PA-CDs) to detect NO_2^- via traditional diazotization, which is fabricated by a high-efficiency, one-pot hydrothermal route utilizing *m*-phenylenediamine as the only precursor. Research into the mechanism revealed that unique aromatic primary amines (Ar-NH_2) were selectively diazotized by NO_2^-, which resulted in fluorescence quenching in a linear relationship. Hence, the nanosensor based on PA-CDs displayed a sensitive and selective method to quench NO_2^- with two good linear range of 0.05–1.0 μM and 1.0–50 μM with a low detection limit of 7.1 nM. In addition, the PA-CDs exhibited bright green fluorescence, high quantum yield (20.1%) and photostability, and strong anti-interference ability in different environments. As far as we know, the PA-CDs reported here are the simplest fluorescent probes that can be used to determine the presence of nitrite ions in environmental water and biological samples. Thus, this method possesses great potential for the selective detection of NO_2^- in real samples and to replace the expensive experiments currently used in conventional methods.

Experimental

Materials

m-Phenylenediamine was purchased from Aladdin Chemistry Co., Ltd. (Shanghai, China). Analytical-grade reagents $NaNO_2$, $NaNO_3$, NaF, NaCl, NaBr, NaI, Na_2S, Na_2SO_4, Na_2SO_3, Na_2CO_3, $NaHCO_3$, Na_3PO_4, Na_2HPO_4, NaH_2PO_4, $FeCl_3$, $FeCl_2$, $MnCl_2$, $CaCl_2$, $BaCl_2$, $ZnCl_2$, $NiCl_2$, $CoCl_2$, $CdCl_2$, $MgCl_2$, citric acid, and ethanol were purchased from Sinopharm Group Co., Ltd. (Shanghai, China). Fetal bovine serum was procured from BioInd (Israel). All reagents were used as received without further purification. Ultrapure water prepared using an Ulupure (Sichuan, China) water purification system was used for all aqueous solutions throughout the study. The 2000 Da cutoff membranes and 0.22 μm pore diameter microporous membrane were purchased from Shanghai Yuanye Bio-Technology Co., Ltd. (Shanghai, China).

Instrumentation

Transmission electron microscopy (TEM) was performed by a copper grid coated with thin films of carbon on a Tecnai G2 F20 microscope (FEI Co., USA) at an accelerating voltage of 200 kV. Fourier-transform infrared spectra (FT-IR) were obtained for KBr pellets on Frontier-PerkinElmer FT-IR spectrometer from 4000 to 600 cm^{-1}. Raman spectra (from 1000 to 2000 cm^{-1}) were measured on Renishaw inVia confocal Raman spectrometers excited by 532 nm laser with a visible grating (1800 l/mm). UV−vis absorption spectra were obtained on a UV-3600 UV-VIS-NIR spectrophotometer (Shimadzu, Japan) by a quartz cuvette with 1 cm path length. Fluorescence excitation and emission spectra were recorded on a Hitachi F-4600 fluorescence spectrophotometer with a scan rate of 240 nm/min, which utilized a Xenon lamp of 1/5 nm slit width and equipped by a quartz cuvette with an optical path length of 1 mm; the excitation (Ex) and emission wavelengths (Em) were 395 nm and 490 nm, respectively. X-ray photoelectron spectroscopy (XPS) survey data were obtained by a Thermo Scientific ESCALAB 250Xi equipped with an Al Kα X-ray source (1487.2 eV); the analysis chamber was 8×10^{-8} mbar and the X-ray spot was 650 μm. Zeta potential of the PA-CDs aqueous solution was measured by a Zetasizer Nano ZS series (Malvern Instruments, UK) with a laser wavelength of 633 nm and a detection angle of 173° at 25 °C. Fluorescent photographs were taken by a SONY DSC-W800 with ZF-20D hand-held UV lamp (Shanghai, China) under excitation at 365 nm.

Preparation of carbon quantum dots

First, 0.2160 g *m*-phenylenediamine (2 mmol) was dispersed in 20 mL ethanol, and then the solution was transferred into a Teflon-lined stainless steel autoclave and heated to 180 °C for 8 h. After the autoclave was allowed to cool, the resulting solution was centrifuged at 9000 rpm for 10 min to remove solids. After ethanol was removed by a rotary evaporator, the acquired product was ultrasonically dispersed in ultrapure water. Next, the obtained solution was dialyzed through a dialysis membrane (MWCO = 2000 Da) for 24 h after filtering by a

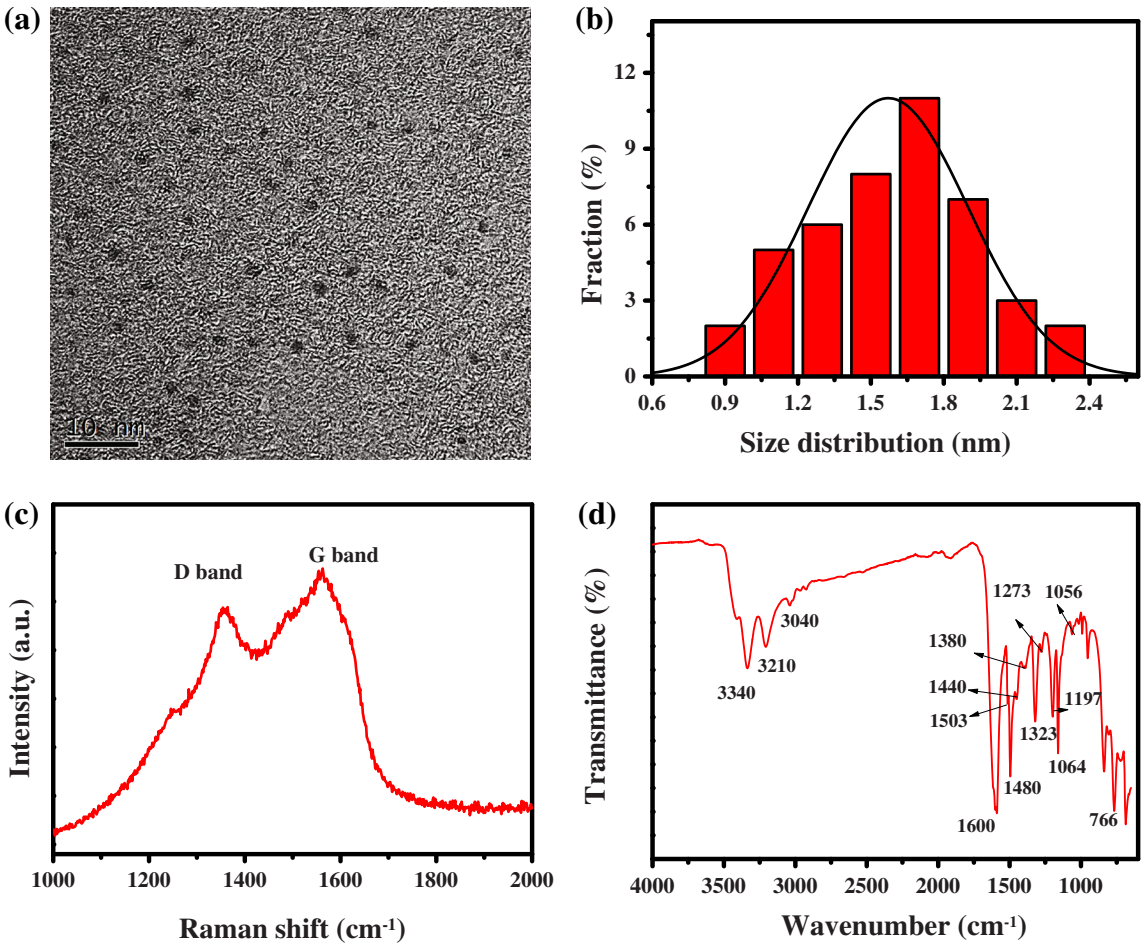

Fig. 1 **a** TEM image, **b** diameter distribution, **c** Raman spectra, and **d** FT-IR spectra of the PA-CDs

0.22-μm pore diameter microporous membrane, and the final PA-CD solid sample was obtained through freeze drying.

Nitrite (NO_2^-) sensing procedures

Various concentrations of NO_2^- (100 μL each) were added into a mixture of 400 μL PA-CD solution (0.1 mg/mL) and 3.5 mL disodium hydrogen phosphate-citrate buffer (pH = 2.0). And then emission spectra were collected and analyzed on a fluorescence spectrophotometer. Using this same method, selectivity experiments were performed by using 100 μL of other inorganic ion or metal ion solutions instead of NO_2^-. The fluorescence response of the PA-CDs was analyzed towards different interfering anions. Competition experiments were carried out with the subsequent addition of 100 μM NO_2^- basis on selectivity experiments. Complex real samples (such as tap water and serum samples) were used to evaluate the feasibility and applicability of the proposed analytical methodology. The tap water and serum samples were diluted (200-fold) before sensing NO_2^-. The obtained samples were spiked with a series of concentrations of standard NO_2^- solution.

Results and discussion

Characterization of PA-CDs

TEM images were used to characterize the morphology and size of PA-CDs (Fig. 1a), and the nanoparticles displayed smooth surface morphologies and uniform spherical nanoparticles with an average diameter of approximately 1.57 nm (Fig. 1b). Raman spectra confirmed that the PA-CDs were partially graphitized, and G and D band signals were observed at 1563 and 1354 cm^{-1}, respectively. The intensity of the G band was greater than the D band (Fig. 1c) which indicated that the as-prepared PA-CDs had a graphite-like structure.

The surface functional groups of PA-CDs were characterized through FTIR spectroscopy (Fig. 1d). The bands at 3340 and 3210 cm^{-1} represented the symmetrical and asymmetrical stretching vibrations of NH_2, respectively. The sharp peak at 1600 cm^{-1} indicated the bending vibrations of N–H, and the out-of-plane bending vibration of N–H at 766 nm was also observed, which demonstrated that many primary amines were present on the surface of PA-CDs. Furthermore, the vibration band at 3040 cm^{-1} was attributed to the Ar–H stretching

frequency. The absorption peaks at 1503, 1487, and 1440 cm^{-1} were attributed to aromatic C=C stretching vibrations. The absorption peaks at 1380, 1323, and 1273 cm^{-1} were identified as aromatic δ_{C-N}. Meanwhile, an additional peak at 1056 cm^{-1} represented C−O stretching. From the above FTIR characteristics, it can be concluded that aromatic primary amino groups were present on the surface of the nanospheres, which demonstrates that *m*-phenylenediamine molecules remained on the surface of PA-CDs.

The elemental composition and chemical valence states of PA-CDs were determined by X-ray photoelectron spectroscopy (XPS). The survey spectrum of PA-CDs in Fig. 2 a indicates the presence of C 1s (285 eV), N 1s (400 eV), and O 1s (533 eV). Figure 2 b shows the high-resolution C 1s XPS spectrum, which can be separated into three peaks, which correspond to sp^2 hybridized carbon atoms in C–C/C=C (284.5 eV), sp^3 hybridized carbon atoms in C−N/C−O (285.6 eV), and carbonyl carbons (C=O) at 287.8 eV [25]. The N 1s spectrum (Fig. 2c) reveals three component peaks at 398.6 eV (pyridinic Ns), 399.5 eV (1°/2° amino Ns), and 400.3 eV (pyrrolic Ns) [26]. The O 1s XPS spectrum (Fig. 2d) has two peaks at 531.6 eV and 533 eV, which likely originate from C=O and C−O [27]. Based on the XPS analysis, it is reconfirmed that the polar functional groups present on the surface of PA-CDs are aromatic primary amino groups. Moreover, the zeta potential (+ 19.5 mV) of PA-CDs in aqueous solution (see Electronic Supplementary Material (ESM) Fig. S1) indicated good dispersibility and solubility in water or acidic solution, likely because of many amino groups on the surface of PA-CDs.

Optical properties of the PA-CDs

The optical properties of the as-obtained PA-CDs were analyzed by UV−vis absorption and fluorescence spectroscopy. The UV−vis spectral peaks at 285 nm and 391 nm were attributed to the aromatic sp^2 π–π* transition and the n–π* transition of the C=O/C–N bonds on the surface of doped PA-CDs, respectively (Fig. 3a). In Fig. 3 b, the fluorescence emission spectra were recorded at an excitation wavelength that varied from 335 to 425 nm, and a significant excitation-independent mode with an emission maximum at 490 nm was observed, which demonstrated that the PA-CDs possessed only one specific and dominant emission mode. Furthermore, the fluorescence excitation spectra manifested an excitation peak centered at 395 nm, which is consistent with the absorption peak at 391 nm. This indicates that the surface structures and states were presumably responsible for the emission at 490 nm. The quantum yield

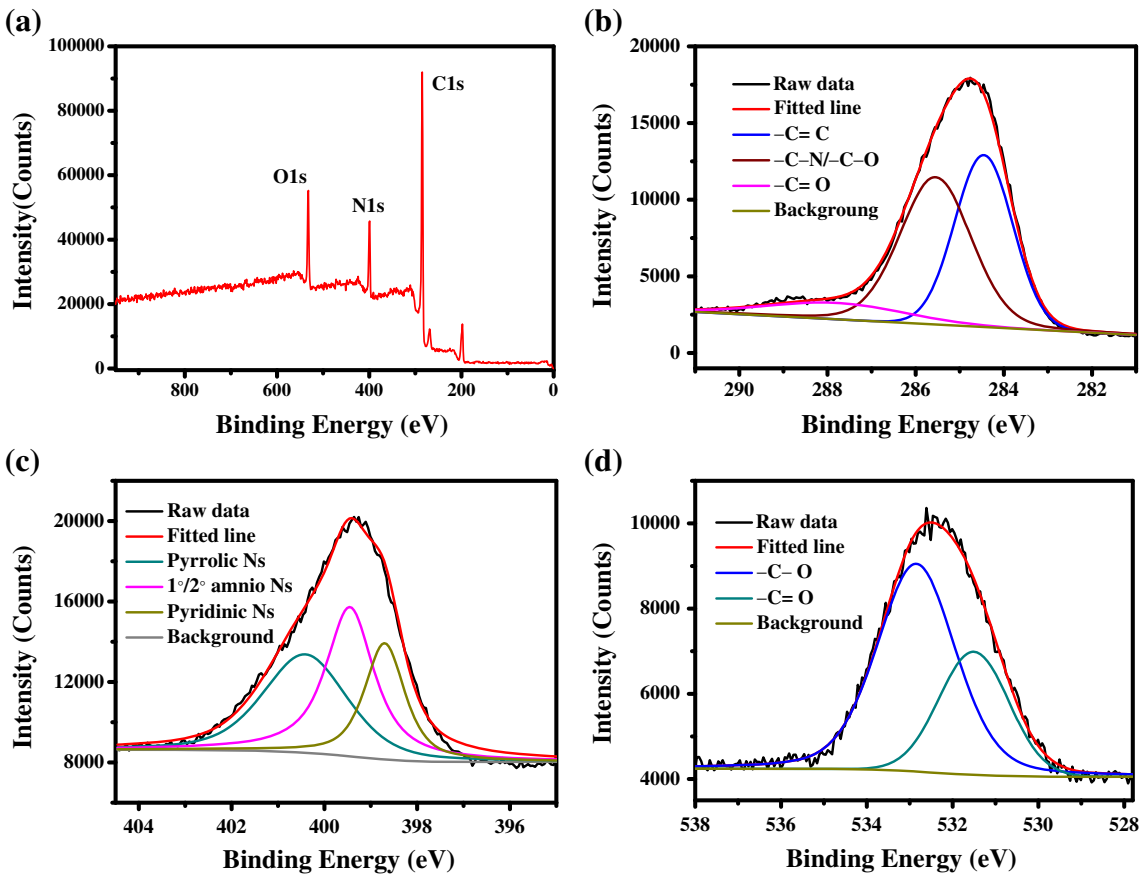

Fig. 2 **a** Full-survey XPS spectrum of PA-CDs. **b** C 1s. **c** N 1s. **d** O 1s deconvolution spectra

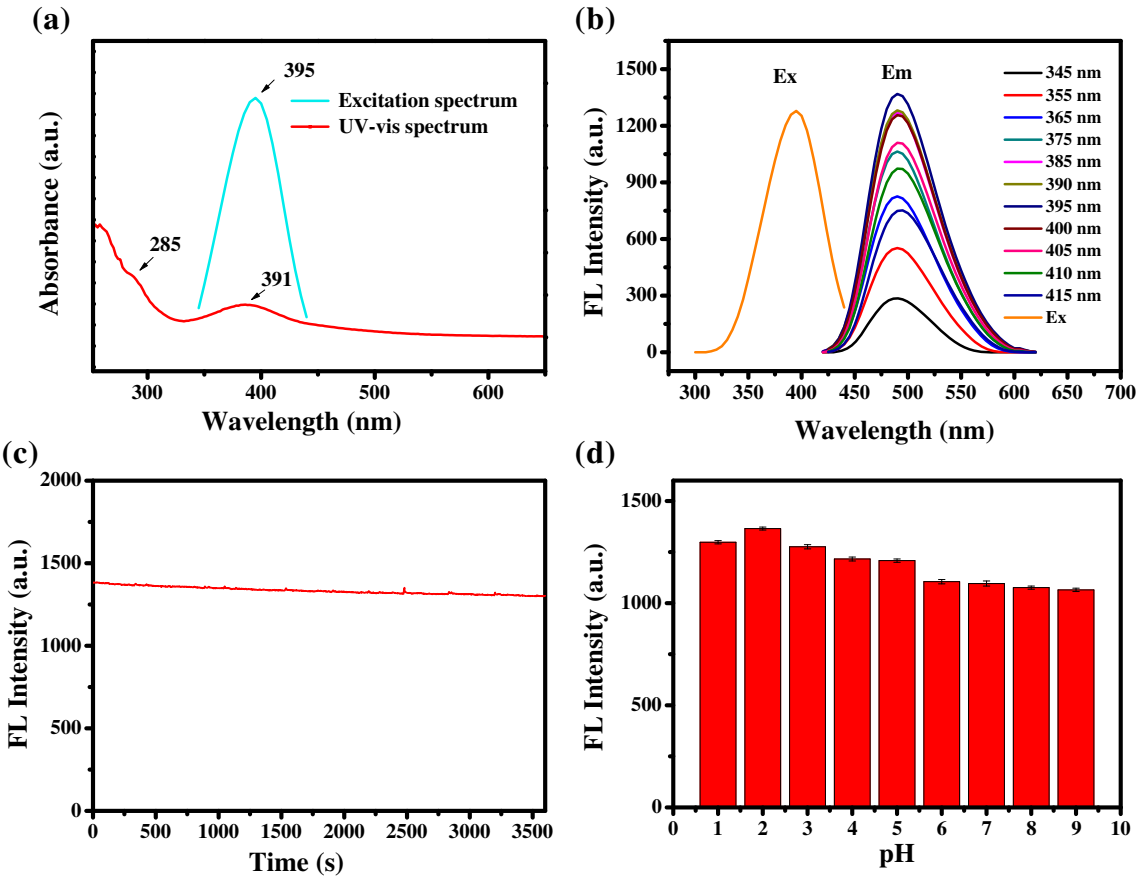

Fig. 3 **a** UV−vis spectrum and excitation spectra. **b** Fluorescence emission spectra at various excitation wavelengths (from 345 to 415 nm). **c** Fluorescence intensity variation of the PA-CDs under uninterrupted irradiation by a 150W Xenon lamp (Ex = 395 nm) for 60 min. **d** Fluorescence intensity (Ex = 395 nm, Em = 490 nm) variation at different pH values

(QY) of PA-CDs in aqueous media was determined to be 20.1% using quinoline sulfate as the standard, which demonstrated that the PA-CDs could potentially be utilized as highly sensitive nanosensors for NO_2^- detection.

A photobleaching experiment was performed to examine the photostability of PA-CDs (Fig. 3c). The fluorescent intensity attenuated and decreased slightly after continuous and uninterrupted irradiation by a 150W Xenon lamp (Ex = 395 nm) for 60 min, demonstrating that the as-fabricated PA-CDs possessed excellent photostability against photobleaching organic probes. Moreover, the fluorescence stability of PA-CDs under various circumstances was also investigated. Interestingly, the fluorescence intensity (Ex = 395 nm, Em = 490 nm) fluctuated as the pH increased from 2 to 9, possibly due to the protonation-deprotonation of external amino groups on the surface of the PA-CDs (Fig. 3d). Furthermore, the response of the PA-CD analysis platform towards NO_2^- at different pH values was investigated, which showed that the fluorescence quenching efficiency was inversely proportional to the pH, and there was no response in either neutral or alkaline conditions (ESM Fig. S2). Aromatic amine diazotization may occur under strongly acidic conditions, and this reaction was likely responsible for the above experimental result [28]. Considering the influence of strong acid on the analytical sample, a buffer system (pH = 2) was employed throughout the experiment. Moreover, whether NO_2^- was present or not, no fluorescence response change was identified in the disodium hydrogen phosphate-citrate buffer solution, which indicated that the buffer did not interfere with NO_2^- detection (ESM Fig. S3). Additionally, the stability of the nanoprobe was also examined under high ionic concentrations up to 1 M NaCl, and the fluorescence intensity of the PA-CDs remained nearly constant (ESM Fig. S4), which further demonstrated high photostability and anti-interface ability of PA-CDs.

NO_2^- ion sensing capability of the PA-CDs

A PA-CD concentration of 0.01 mg/ml was eventually chosen for the quantitative detection of NO_2^-. The fluorescence intensity at 490 nm continuously decreased as the concentration of NO_2^- increased (Fig. 4a). As shown in Fig. 4 b and c, the quenching efficiency (F_0/F) versus various concentration of NO_2^- displayed two excellent linear ranges, i.e., 0.05–1.0 μM ($R^2 = 0.992$) and 1.0–50 μM ($R^2 = 0.994$), demonstrating that the PA-CDs could be successfully used as nano-fluorophores

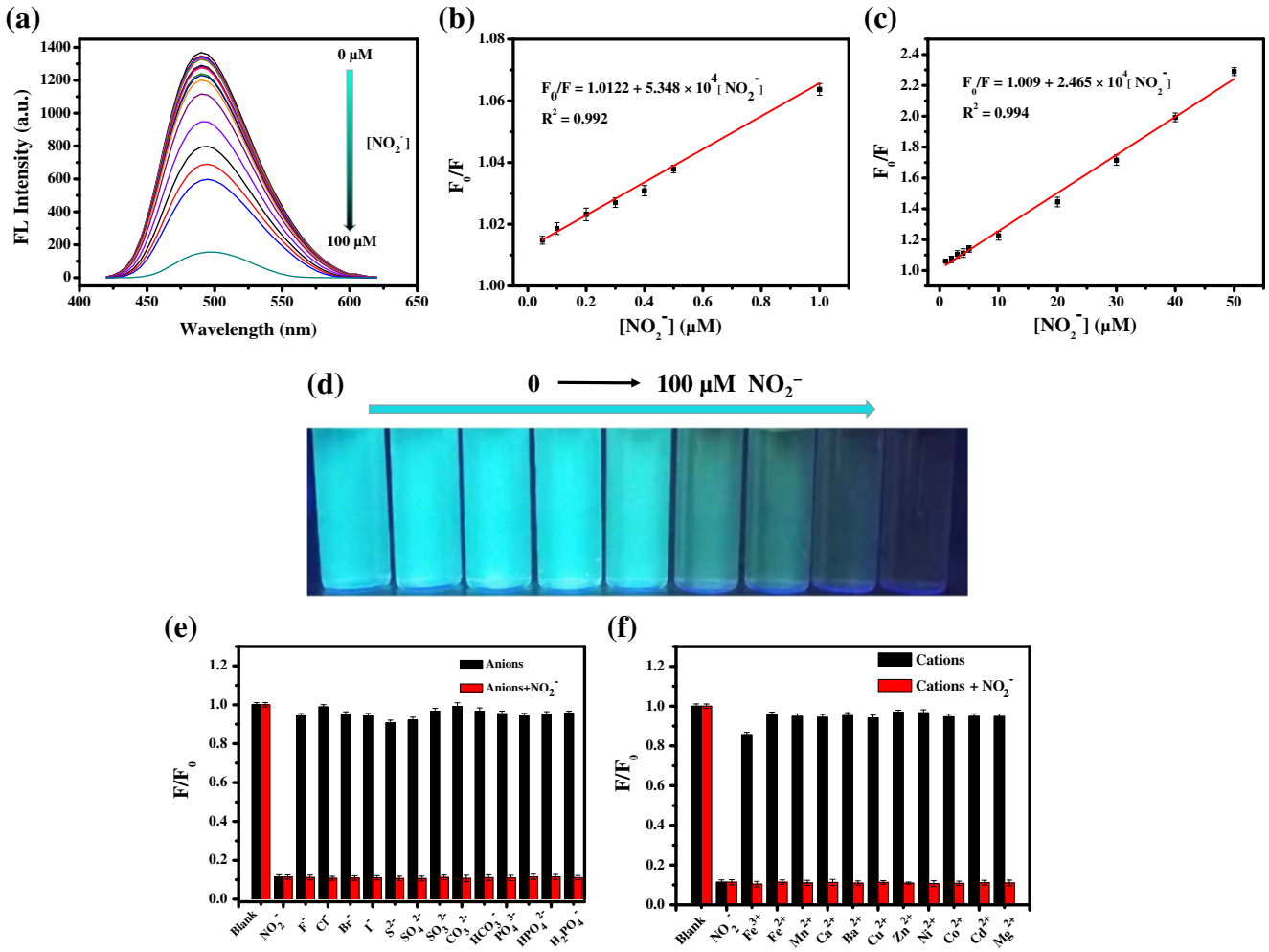

Fig. 4 **a** Fluorescence emission spectra of PA-CDs (0.01 mg/mL) with various amounts of NO_2^- (0–100 μM). **b** and **c** Stern−Volmer plot of PA-CDs quenched by NO_2^- within the range of 0.05–1.0 μM and 1.0–50 μM, where F_0 and F are fluorescence intensities of the PA-CDs in the absence and presence of NO_2^-, respectively. **d** Photographs of PA-CDs with gradually increasing concentrations of NO_2^- under a 365 nm UV irradiation. **e** Fluorescence intensity variation (F/F_0) of PA-CDs with different anion ions ([NO_2^-] = 100 μM, [other interference anions] = 400 μM, black bar) and upon the subsequent addition of 100 μM NO_2^- (red bars). **f** Fluorescence intensity variation of PA-CDs towards various cations ([NO_2^-] = 100 μM, [other interference metal ions] = 200 μM, black bars) and upon the subsequent addition of 100 μM NO_2^- (red bars)

to detect trace amounts of NO_2^-. The concentration dependence of fluorescence quenching efficiency (F_0/F) can be fitted into $(F_0/F) = 1.012 + 5.348 \times 10^4$ [NO_2^-] (0.05–1.0 μM) and $(F_0/F) = 1.009 + 2.465 \times 10^4$ [NO_2^-] (1.0–50 μM), respectively, by the Stern−Volmer equation:

$$F_0/F = 1 + K_{SV}[NO_2^-]$$

where F_0 and F are the fluorescence intensity of the PA-CDs at 490 nm in the absence and presence of NO_2^-, respectively; [NO_2^-] is the concentration of NO_2^-; and K_{SV} is the Stern−Volmer constant.

The quantitative detection equation revealed two wide linear range (0.05–1.0 μM and 1.0–50 μM) with a low detection limit of 7.1 nM, demonstrating the promising applicability of PA-CDs to the sensitive and trace detection of NO_2^-. And the detection limit (7.1 nM) was estimated based on the regression curve of $(F_0/F) = 1.012 + 5.348 \times 10^4$ [NO_2^-] according to the 3σ (signal-to-noise) ratio. Meanwhile, the fluorescence intensity of PA-CDs was gradually quenched and attenuated as the NO_2^- concentration increased from 0 to 100 μM, and these samples were photographed under a 365 nm UV lamp (Fig. 4d). These results indicated that the NO_2^- could be simply visualized by the naked eye based on fluorescence response.

To determine the practicality of the PA-CDs as fluorescent nanosensors, it is crucial to explore their selectivity and anti-interference ability in an intricate real system. Hence, some anion ions (NO_2^-, NO_3^-, F^-, Cl^-, Br^-, I^-, S_2^-, SO_4^{2-}, SO_3^{2-}, CO_3^{2-}, HCO_3^-, PO_4^{3-}, HPO_4^{2-}, and $H_2PO_4^-$) were used. As shown in Fig. 4 d, the fluorescence intensity (black bar) remained nearly the same, indicating the high selectivity of PA-CDs to NO_2^- against other anions, because there is a nonspecific response

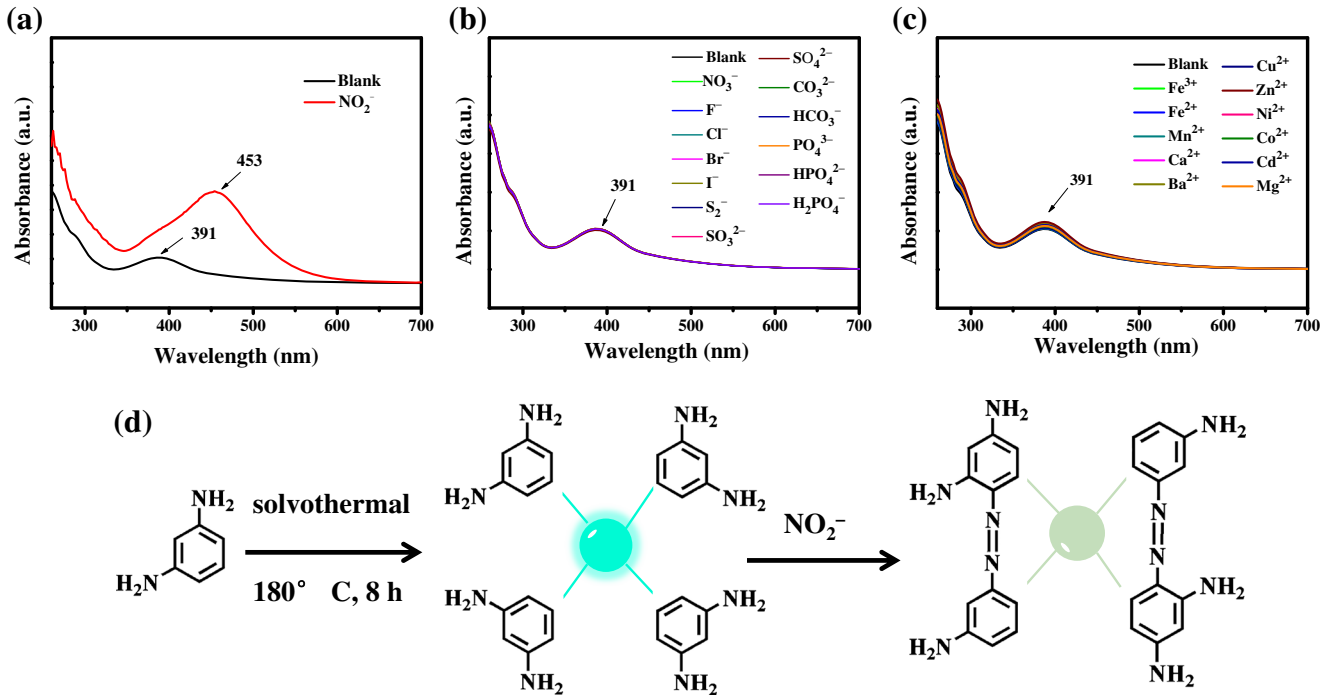

Fig. 5 **a** UV−vis absorption spectra of PA-CDs in the absence and presence of NO_2^-. **b** UV−vis absorption spectra of PA-CDs and after the addition of various anions. **c** UV−vis absorption spectra of PA-CDs and after the addition of various cations. **d** Schematic illustration of the preparation of the nanosensor and a suggested fluorescence quenching mechanism of the nanosensor in the presence of NO_2^- (not to scale)

between functional groups and other anions. Anti-interference experiments (red bars, Fig. 4e) were conducted by subsequently adding 100 μM NO_2^- to each solution, where the concentration ratio of NO_2^- to other anion is 1:4. That implied that the most anions can coexist in the solution for the NO_2^- detection without any interference. To further demonstrate the specificity of this method for NO_2^- detection, a similar experiment was performed to evaluate common cations (Fe^{3+}, Fe^{2+}, Mn^{2+}, Ca^{2+}, Ba^{2+}, Cu^{2+}, Zn^{2+}, Ni^{2+}, Co^{2+}, Cd^{2+}, Mg^{2+}) in the analytical system with a NO_2^- to interference cation concentration ratio of 1:2 (Fig. 4f). The fluorescence response showed negligible interference to the selectivity of PA-CDs, which was attributed to the loose chelation between metal ions and functional groups.

The selectivity and anti-interference experiment suggested that the PA-CDs had a high selectivity to NO_2^- against both anions and metal ions. Various ions can coexist in an analysis system with the NO_2^- without interfering with the detection of NO_2^-. That further demonstrated the feasibility of using the PA-CDs to sense NO_2^- in interfering biological and physiological environments.

Table 1 Fluorescence recovery experiments of NO_2^- from real tap water and serum samples

Sample	Added (μM)	Found (μM)	Recovery (%)	RSD (%)
Tap water	0.6	0.63	105.0	3.2
	2.4	2.43	101.3	1.5
	6.0	5.95	99.2	2.1
	24.0	23.80	99.2	2.6
Serum	0.6	0.65	108.3	3.0
	2.4	2.49	103.8	2.8
	6.0	5.81	96.7	1.4
	24.0	22.17	92.3	0.7

The quenching mechanism of PA-CD nanosensor towards nitrite

The possible quenching mechanism of the PA-CD nanosensor towards nitrite is proposed to proceed via a diazotization mechanism. This is confirmed by extensive reports that primary arylamines can be diazotized by NO_2^- to form diazonium salts in strongly acidic media [28–30]. The surface aromatic primary ammonia groups of the PA-CDs were first diazotized by NO_2^- in acidic medium (reaction 1), which then subsequently formed an azo compound (reaction 2) (ESM Fig. S5) [31–33]. The peculiar molecular structure of *m*-phenylenediamine is responsible for the subsequent coupling reaction. The corresponding fluorescence quenching mechanism may be ascribed to the formation of an azo compound. To verify the production of an azo compound, UV–vis spectra were used to evaluate the absorption fluctuation after diazotization. The absorption peak of PA-CDs after participating in

Table 2 Comparison of a variety of reported nanoprobes for the determination of NO_2^- with diverse ways recently

Sensor	Detective method	Sample	Detection range (μmol/L)
Au-PtNPs/PyTS-NG	Electrochemistry	Water/ham	0.5–1621
GC/AuMNNSs	Electrochemistry	Water	0.4–806.6
Hydrogel	Colorimetry	Ham	10–5000
Fe_3O_4-SiO_2-PAMAM-PPD-NAS	Fluorescence	Beverages	0.35–11.76
Au NPs	Raman scattering	Saliva	20–120
CDs	Chemiluminescence	Water/milk	0.1–10
PA-CDs	Fluorescence	Water/serum	0.05–50

the coupling reaction with NO_2^- exhibited a 62 nm red shift (from 391 to 453 nm) (Fig. 5a), which was attributed to the formation of an azo group (N=N) via a diazo coupling reaction [34]. However, there were no spectral shifts for other anions (Fig. 5b) and cations (Fig. 5c), and the vertically offset (anions, < 3.6%; cations, < 16.4%) did not exhibit significant change, which demonstrated strong anti-interference ability for nitrite detection by PA-CDs. Meanwhile, the color change of PA-CD solution may also arise from the formation of an azo compound (ESM Fig. S6). Furthermore, the FTIR spectroscopy of PA-CDs after the diazo coupling reaction with NO_2^- was also investigated (ESM Fig. S7). It indicated that the aromatic amine peaks at 3340 and 3210 cm^{-1} were greatly weakened and nearly vanished, while a new peak at 1687 cm^{-1} appeared which was attributed to the formation of a diazo group [35]. These FTIR spectral differences further demonstrated that the surface aromatic primary amine groups of the PA-CDs were transformed into azo complexes by NO_2^- in the acidic medium. Therefore, it is speculated that the fluorescence quenching of the PA-CDs is predominantly ascribed to a photoinduced electron transfer process from the excited state of the PA-CDs to the azo compounds on their surface (Fig. 5d).

NO_2^- ion sensing performance of the PA-CDs in real sample

In light of the remarkable sensing performance and excellent anti-interference ability of PA-CDs, the proposed PA-CDs were used as an analytic platform to detect NO_2^- in different water samples. Tap water and serum were chosen as models for environmental and biological samples, respectively, by spiking them with four different nitrite concentrations, which were prepared to be quantitatively analyzed using the PA-CDs.

A series of concentrations of a standard NO_2^- solution were added to tap water samples and were then directly subjected to the PA-CD sensing system. They were allowed to interact with each other for 60 min, and then the fluorescence intensity was recorded to evaluate the recovery rate and accuracy using the above linear fitting equation for fluorescence quenching. Each experiment was performed three times, and the values reported in Table 1 are the mean concentrations accompanied by their relative standard deviation (RSD). Interestingly, the concentration values determined using the PA-CDs are very consistent with the spiked concentrations. The fluorescence recovery of tap water with different NO_2^- concentrations was greater than 99.2%, and the RSD was less than 3.2%, which demonstrated this method can detect trace amounts of nitrites in food and complex environments.

In addition, while there are many interference components in the serum sample (fetal bovine serum), the recovery was more than 92.3%, and the RSD was less than 3.0%, which confirmed that the PA-CD method can be applied to track trace amounts of nitrite in biological fields and provide effective information for clinical diagnoses. The high fluorescence recoveries and excellent detection precision further verify the dependability and feasibility of using PA-CDs as a sensing platform to analyze trace amounts of nitrites in complex environmental and biological samples.

The detection of nitrite ion has been performed by a variety of methods, including combinatorial electrochemistry by Au-PtNPs/PyTS-NG [36] and GC/AuMNNSs [37], colorimetry by hydrogel [38], fluorescence by Fe_3O_4-SiO_2-PAMAM-PPD-NAS [39], Raman scattering by AuNPs [40], and chemiluminescence by CDs [41]. However, there are few reports of fluorescent carbon quantum dots to accomplish nitrite ion detection, and the analytical performances of proposed sensor and previously reported nitrite sensors are summarized and compared in Table 2. The sensitivity and selectivity of PA-CDs illustrate a comparable detection range, further confirming the potential application of PA-CDs for nitrite detection.

Conclusions

A novel nitrite nanosensor was fabricated with *m*-phenylenediamine by a high-efficiency, one-pot hydrothermal route, which demonstrated a facile, economical, and efficient strategy to prepare carbon quantum dots. The synthesized PA-CDs demonstrated an excellent linear relationship in two wide concentration range (0.05–1.0 μM and 1.0–50 μM) with a low detection limit of 7.1 nM, indicating that this sensor was a sensitive, accurate, specific, and reliable tool for the detection

of nitrite ions. Importantly, we further confirmed that our proposed method could successfully track NO_2^- in environmental water and serum samples in close agreement with known spiked concentrations. A classical diazo-reaction mechanism was used to ensure the outstanding sensitivity and selectivity to NO_2^- in various measuring environments. This provides a new methodology to construct carbon quantum dots and improve their anti-interference abilities and chemical stability from various interfering environmental factors. This work broadens the application of carbon quantum dots as nanosensors, and provides a prospective use for carbon quantum dots derived from aromatic primary amines in practical applications. The proposed methodology in this work can be extended to fabricate novel nanosensors for other analytes in various fields.

Funding information This research was supported by Shaanxi Provincial Natural Science Basic Research Project, China (2018JM2037) and Shaanxi Provincial Natural Science Basic Research Program - General Project (Youth) "2019JQ-461." This study was also supported by China postdoctoral science foundation on the 61st project (2017M613190).

Compliance with ethical standards

Conflict of interest The authors declare that they have no conflicts of interests.

References

1. Liu L, Ma Q, Liu Z, Li Y, Su X. Detection of trace nitrite in waters using a QDs-based chemiluminescence analysis system. Anal Bioanal Chem. 2014;406(3):879–86.
2. Ma Y, Wang Y, Xie D, Gu Y, Zhang H, Wang G, et al. NiFe-layered double hydroxide nanosheet arrays supported on carbon cloth for highly sensitive detection of nitrite. ACS Appl Mater Interfaces. 2018;10(7):6541–51.
3. Xiong Y, Zhu DQ, Duan CF, Guan YF. Small-volume fiber-optic evanescent-wave absorption sensor for nitrite determination. Anal Bioanal Chem. 2010;396(2):943–8.
4. Lijinsky W, Epstein SS. N-Nitrosamines as environmental carcinogens. Nature. 1970;225(5227):21–3.
5. Wang QH, Yu LJ, Liu Y, Lin L, Lu RG, Zhu JP, et al. Methods for the detection and determination of nitrite and nitrate: a review. Talanta. 2017;165:709–20.
6. Yue R, Lu Q, Zhou YK. A novel nitrite biosensor based on single-layer graphene nanoplatelet-protein composite film. Biosens Bioelectron. 2011;26(11):4436–41.
7. Haldorai Y, Hwang SK, Gopalan AI, Huh YS, Han YK, Voit W, et al. Direct electrochemistry of cytochrome c immobilized on titanium nitride/multi-walled carbon nanotube composite for amperometric nitrite biosensor. Biosens Bioelectron. 2016;79:543–52.
8. Møller JKS, Skibsted LH. Nitric oxide and myoglobins. Chem Rev. 2002;102(4):1167–78.
9. Yao M, Roberts DD, Isenberg JS. Thrombospondin-1 inhibition of vascular smooth muscle cell responses occurs via modulation of both cAMP and cGMP. Pharmacol Res. 2011;63(1):13–22.
10. Sheu JR, Hung WC, Su CH, Lin CH, Lee LW, Lee YM, et al. The antiplatelet activity of Escherichia coli lipopolysaccharide is mediated through a nitric oxide/cyclic GMP pathway. Eur J Haematol. 1999;62(5):317–26.
11. Zhang HM, Kang SH, Wang GZ, Zhang YX, Zhao HJ. Fluorescence determination of nitrite in water using prawn-shell derived nitrogen-doped carbon nanodots as fluorophores. ACS Sensors. 2016;1(7):875–81.
12. Ghanei-Motlagh M, Taher MA. A novel electrochemical sensor based on silver/halloysite nanotube/molybdenum disulfide nanocomposite for efficient nitrite sensing. Biosens Bioelectron. 2018;109:279–85.
13. Miao P, Shen M, Ning LM, Chen GF, Yin YM. Functionalization of platinum nanoparticles for electrochemical detection of nitrite. Anal Bioanal Chem. 2011;399(7):2407–11.
14. Yin XX, Chen QF, Song HL, Yang M, Wang HY. Sensitive and selective electrochemiluminescent detection of nitrite using dual-stabilizer-capped CdTe quantum dots. Electrochem Commun. 2013;34:81–5.
15. He LJ, Zhang KG, Wang CJ, Luo XL, Zhang SS. Effective indirect enrichment and determination of nitrite ion in water and biological samples using ionic liquid-dispersive liquid-liquid microextraction combined with high-performance liquid chromatography. J Chromatogr A. 2011;1218(23):3595–600.
16. Zheng P, Kasani S, Shi X, Boryczka AE, Yang F, Tang H, et al. Detection of nitrite with a surface-enhanced Raman scattering sensor based on silver nanopyramid array. Anal Chim Acta. 2018;1040:158–65.
17. Brandao GC, Matos GD, Pereira RN, Ferreira SLC. Development of a simple method for the determination of nitrite and nitrate in groundwater by high-resolution continuum source electrothermal molecular absorption spectrometry. Anal Chim Acta. 2014;806:101–6.
18. Dong SC, Guan WJ, Lu C. Quantum dots in organo-modified layered double hydroxide framework-improved peroxynitrous acid chemiluminescence for nitrite sensing. Sensors Actuators B Chem. 2013;188:597–602.
19. Kudr J, Richtera L, Xhaxhiu K, Hynek D, Heger Z, Zitka O, et al. Carbon dots based FRET for the detection of DNA damage. Biosens Bioelectron. 2017;92:133–9.
20. Shangguan J, Huang J, He D, He X, Wang K, Ye R, et al. Highly Fe^{3+}-selective fluorescent nanoprobe based on ultrabright N/P codoped carbon dots and its application in biological samples. Anal Chem. 2017;89(14):7477–84.
21. Chen X, Gong F, Cao Z, Zou W, Gu T. Highly cysteine-selective fluorescent nanoprobes based on ultrabright and directly synthesized carbon quantum dots. Anal Bioanal Chem. 2018;410(12):2961–70.
22. Gao WL, Song HH, Wang X, Liu XQ, Pang XB, Zhou YM, et al. Carbon dots with red emission for sensing of Pt^{2+}, Au^{3+}, and Pd^{2+} and their bioapplications in vitro and in vivo. ACS Appl Mater Interfaces. 2018;10(1):1147–54.
23. Zhao L, Li HY, Xu Y, Liu HC, Zhou TY, Huang N, et al. Selective detection of copper ion in complex real samples based on nitrogen-doped carbon quantum dots. Anal Bioanal Chem. 2018;410(18):4301–9.
24. Wen L, Diao HP, Chang HH, Wang HJ, Li TT, Wei WL. Green synthesis of carbon dots from rose-heart radish and application for Fe^{3+} detection and cell imaging. Sensors Actuators B Chem. 2017;241:190–8.
25. Chen J, Wei JS, Zhang P, Niu XQ, Zhao W, Zhu ZY, et al. Red-emissive carbon dots for fingerprints detection by spray method: coffee ring effect and unquenched fluorescence in drying process. ACS Appl Mater Interfaces. 2017;9(22):18429–33.
26. Vedamalai M, Periasamy AP, Wang CW, Tseng YT, Ho LC, Shih CC, et al. Carbon nanodots prepared from o-phenylenediamine for sensing of Cu^{2+} ions in cells. Nanoscale. 2014;6(21):13119–25.

27. Jiao Y, Gong XJ, Han H, Gao YF, W. Lu, Liu Y, et al. Facile synthesis of orange fluorescence carbon dots with excitation independent emission for pH sensing and cellular imaging. Anal Chim Acta 2018;1042:125–132.
28. Butler RN. Diazotization of heterocyclic primary amines. Chem Rev. 1975;75(2):241–57.
29. Fanning AT, Bickford GR, Roberts TD. Preparation and diazotization of thioanthranilic acid. Chemistry of 4-oxo-3,4-dihydro-3,1,2-benzothiadiazine. J Am Chem Soc. 1972;94(24):8505–9.
30. Friedman L, Logullo FM. Benzynes via aprotic diazotization of anthranilic acids: a convenient synthesis of triptycene and derivatives. J Am Chem Soc. 1963;85(10):1549.
31. Bailey JE. Determination of unsulfonated aromatic amines in D & C Red No. 33 by the diazotization and coupling procedure followed by reversed-phase liquid chromatographic analysis. Anal Chem. 1985;57(1):189–96.
32. Koukabi N, Otokesh S, Kolvari E, Amoozadeh A. Convenient and rapid diazotization and diazo coupling reaction via aryl diazonium nanomagnetic sulfate under solvent-free conditions at room temperature. Dyes Pigments. 2016;124:12–7.
33. Kunduru KR, Basu A, Tsah T, Domb AJ. Polymer with pendant diazo-coupling functionality for colorimetric detection of nitrates. Sensors Actuators B Chem. 2017;251:21–6.
34. Lei Z, Cole JM, Liu X. Tuning solvatochromism of azo dyes with intramolecular hydrogen bonding in solution and on titanium dioxide nanoparticles. J Phys Chem C. 2013;117(49):26316–23.
35. Qiu JJ, Xiao JQ, Tang BT, Ju BZ, Zhang SF. Facile synthesis of novel disperse azo dyes with aromatic hydroxyl group. Dyes Pigments. 2019;160:524–9.
36. Li Z, An ZZ, Guo YY, Zhang KN, Chen XL, Zhang DX, et al. Au-Pt bimetallic nanoparticles supported on functionalized nitrogen-doped graphene for sensitive detection of nitrite. Talanta. 2016;161:713–20.
37. Viswanathan P, Ramaraj R. Bi-functional sensing capability of gold multi-pod network nanostructures towards nitrite and guanine. Sensors Actuators B Chem. 2018;270:56–63.
38. Nam J, Jung IB, Kim B, Lee SM, Kim SE, Lee KN, et al. A colorimetric hydrogel biosensor for rapid detection of nitrite ions. Sensors Actuators B Chem. 2018;270:112–8.
39. Wang BY, Wu ZL, Qin WD. Polyamidoamine dendrimer-armed fluorescent magnetic nanoparticles for sensitive and selective determination of nitrite in beverages. Sensors Actuators B Chem. 2017;247:774–9.
40. Yang HR, Xiang Y, Guo XY, Wu YP, Wen Y, Yang HF. Diazo-reaction-based SERS substrates for detection of nitrite in saliva. Sensors Actuators B Chem. 2018;271:118–21.
41. Lin Z, Xue W, Chen H, Lin JM. Peroxynitrous-acid-induced chemiluminescence of fluorescent carbon dots for nitrite sensing. Anal Chem. 2011;83(21):8245–51.